Available online at www.sciencedirect.com
SCIENCE DIRECT®
Journal of Nuclear Materials 352 (2006) 22–28
journal of nuclear materials
www.elsevier.com/locate/jnucmat

Atomistic simulation of rapid compression of fractured silicon carbide

A. Romano [a,*], J. Li [b], S. Yip [c,d]

[a] Laboratory for Reactor Physics and Systems Behaviour, Paul Scherrer Institut, OVGA/226, CH5232 Villigen PSI, Switzerland
[b] Department of Materials Science and Engineering, Ohio State University, Columbus, OH 43210, USA
[c] Department of Nuclear Science and Engineering, Massachusetts Institute of Technology, Cambridge, MA 02139, USA
[d] Department of Materials Science and Engineering, Massachusetts Institute of Technology, Cambridge, MA 02139, USA

Abstract

Deformation mechanisms of a crack in silicon carbide under high-rate compression are investigated by molecular dynamics simulation. The penny-shaped crack is in tension throughout the simulation while a variable compression is applied in an in-plane direction. Two different mechanisms of crack-tip response are observed: (1) At low tension, a disordered band forms from the crack surface in the direction orthogonal to the compression, which grows as the compressional force is increased in a manner suggesting a stress-induced transition from an ordered to a disordered phase. Moreover the crack is observed to close. (2) At a tension sufficient to allow the crack to remain open, the compressional stress induces formation of disordered regions along the boundaries of the opened crack, which grow and merge into a band as the compression proceeds. This process is driven by bending of the initial crack, which transforms into a curved slit. This mechanism induces incorporation of fragments of perfect crystal into the disordered band. Similar mechanisms have been experimentally observed to occur in porous SiC under high-strain rate compression.

PACS: 62.20.Mk; 62.50.+p

1. Introduction

Silicon carbide (SiC) is a technologically important material with a variety of applications such as electronic devices and armour systems [1,2]. The nuclear industry foresees application of SiC in structural components like the inner wall of fusion reactors and innovative fuels [3,4]. The high thermal conductivity and melting point and favourable mechanical properties of this material combined with neutron transparency make it a promising candidate for application as inert matrix in advanced fuels for next generation gas reactor and actinide transmutation systems [5].

In view of its utilization in harsh mechanical and thermal environments, several recent studies have been carried out to investigate the mechanical behavior of SiC when fast and large-magnitude compressional deformations are applied. These loading conditions develop in armour structures

* Corresponding author. Tel.: +41 56 310 2084; fax: +41 56 310 2327.
E-mail address: antonino.romano@psi.ch (A. Romano).

0022-3115/$ - see front matter
doi:10.1016/j.jnucmat.2006.02.038

when a penetrator impacts on the material [6]. Moreover, in postulated reactivity-initiated accidents in nuclear reactors, rapid energy injection in the fuel causes high-rate deformations which can yield large local compressional stresses due to the confining effect of the cladding [7].

Recent experiments of high-rate compression and shock wave tests of pre-cracked and granular silicon carbide revealed that cracking of the material and subsequent formation and growth of shear bands accommodate a large fraction of the material deformation (>50%) during fast compression in cylindrical geometries [8,9]. Incorporation of debris inside the shear bands was also observed in some experiments, and mechanisms involving local bending of the crystal have been introduced to explain this failure behavior. Moreover, dynamic tests of silicon carbide fragmentation in unidirectional compression experiments (without lateral constraints) also indicated that nucleation of microcracks subjected to local tensile forces (wing cracks) and inertia dependent crack growth phenomena drive the macroscopic dynamic failure of SiC [10,11].

Despite the large amount of experimental evidence pointing towards the mechanisms of SiC deformation under compression involving both brittle (cracking) and plastic (shear band formation) behaviors, atomistic understanding of these phenomena is not yet available. Therefore, in this study, we apply molecular dynamics (MD) simulation to investigate the mechanisms of deformation of SiC in the presence of a crack when large unidirectional compressional stresses are applied to the material subjected to lateral confinement. The investigation yields atomistic insight into the formation and evolution of localized disordered bands which are the key microstructures governing the mechanical behavior of SiC under compression. Connections are made with microstructures observed in the experiments and with longitudinal stress measurements.

The following section describes the MD methodology adopted to investigate SiC under fast compression. Presentation and discussion of results are reported next. The main findings are summarized in the conclusions.

2. Methodology

The fast compression simulations of pre-cracked SiC have been performed using molecular dynamics. A supercell of ~20 000 atoms was created with 40 and 8 unit cells along the z-axis and the x- and y-axis, respectively (see Fig. 1). A 2D penny-shaped crack was obtained by eliminating atoms located within an elliptical-base tube, with axial axis oriented along the x-direction, centred in the middle of the specimen (see Fig. 1). Since periodic boundary conditions are applied, the simulated system can be thought of as a porous SiC specimen (with nanometer sized pores). The equilibrium lattice constant at $T = 300$ K was selected initially along both the x- and z-axis – i.e., $a_j = 4.32$ Å with $j = x, z$ – while that along the y-axis, a_y, was parametrically varied from 4.5 to 4.9 Å (or equivalently, ε_{yy} was varied from 4% to ~13%), to keep the crack open under the effect of local tensile forces. A modified version of the Tersoff potential [12] was selected to model the interatomic interaction. It should be mentioned that the selection of the cut-off distances for this potential greatly affects its behavior, because upon application of loading to a supercell of atoms unphysical interactions between second neighbour atoms can be triggered (for example, if the cut-off distance is constant, second neighbour Si–Si interactions can be activated upon uniform compression [13]). Therefore, in the Tersoff potential used in this study we opted to

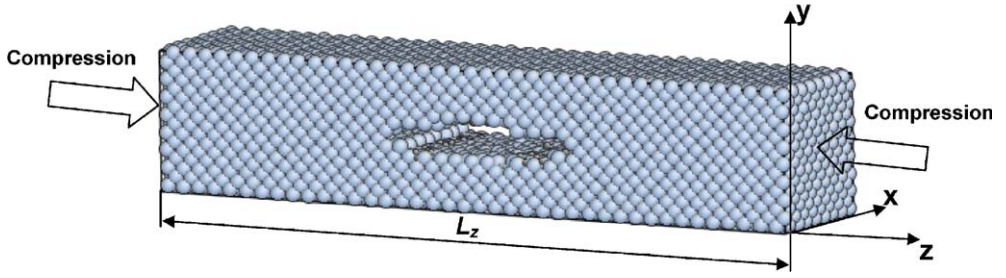

Fig. 1. Reference MD supercell containing a central crack. The coordinate system and direction of applied compression are indicated by arrows.

exclude the Si–Si interactions following the suggestion of Porter et al. in Ref. [13].

The specimens were initially equilibrated by running NVT simulations for ~100 ps to eliminate unfavourable atomic configurations at the crack surface. Subsequently, compressional loads have been applied along the z-axis by rescaling the length of the supercell box, L_z. At each time step, L_z was reduced by $\sim 4 \times 10^{-4}$%, corresponding to a deformation rate of $\sim 50\ \mu s^{-1}$. After rescaling, the system was evolved by running the molecular dynamics algorithm and the new resulting atomic configuration was applied the next compressional step (rescaling of L_z). This procedure was repeated for ~160 ps, a time sufficient to observe the onset of mechanical instabilities and the formation and evolution of microstructures (specifically a disordered band) described in the next section.

3. Results and discussion

In this section we present results of several compressional simulations performed using MD. Specifically, we focus on two deformation mechanisms: development of a disordered band from a crack in Fig. 2 and a similar mechanism involving crack bending and crack surface atomic attrition with subsequent development of a disordered band in Figs. 3 and 4. Fig. 5 reports calculated and measured longitudinal stresses and comparison with experimental measurements is provided.

Fig. 2 shows eight snapshots of the SiC specimen taken at different times during the deformation. The initial dimensions of the unit cell are $a_x = 4.32$ Å, $a_y = 4.725$ Å, and $a_z = 4.32$ Å, respectively, therefore the applied lateral deformation ε_{yy} is 9.38%. The loads applied along the z-axis produce a progressive reduction of the length of the crack, whose surface's atoms carry the highest shear strain. At $t = 43.8$ ps nucleation of local disordered atomic arrangements on the crack surface and around locations of highest shear is observed (Von Mises shear strain ~0.7 compared to ~0.05 for perfect crystal atoms. Note that Fig. 2 uses atom coordination number color encoding [14]). The local disordered nucleus evolves quickly into an extended disordered region which seems to be 'emitted' from the crack surface orthogonally to the direction of the load, at the time the mechanical instability is triggered. As the compression proceeds, the disordered band grows parallel to the direction of the load in a manner resembling a stress-driven amorphization

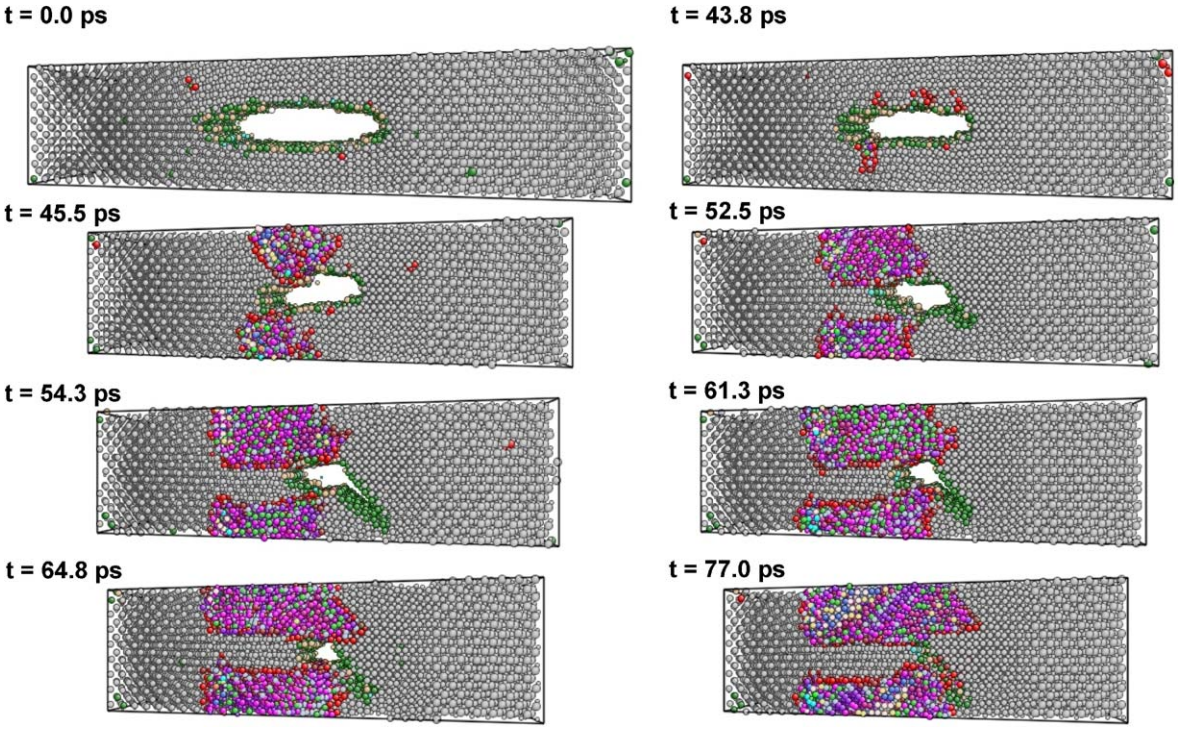

Fig. 2. Snapshots of the specimen with $a_y = 4.725$ Å ($\varepsilon_{yy} = 9.38\%$) showing time evolution of deformation and failure of SiC over 77 ps. A disordered band generates and grows from the crack surface.

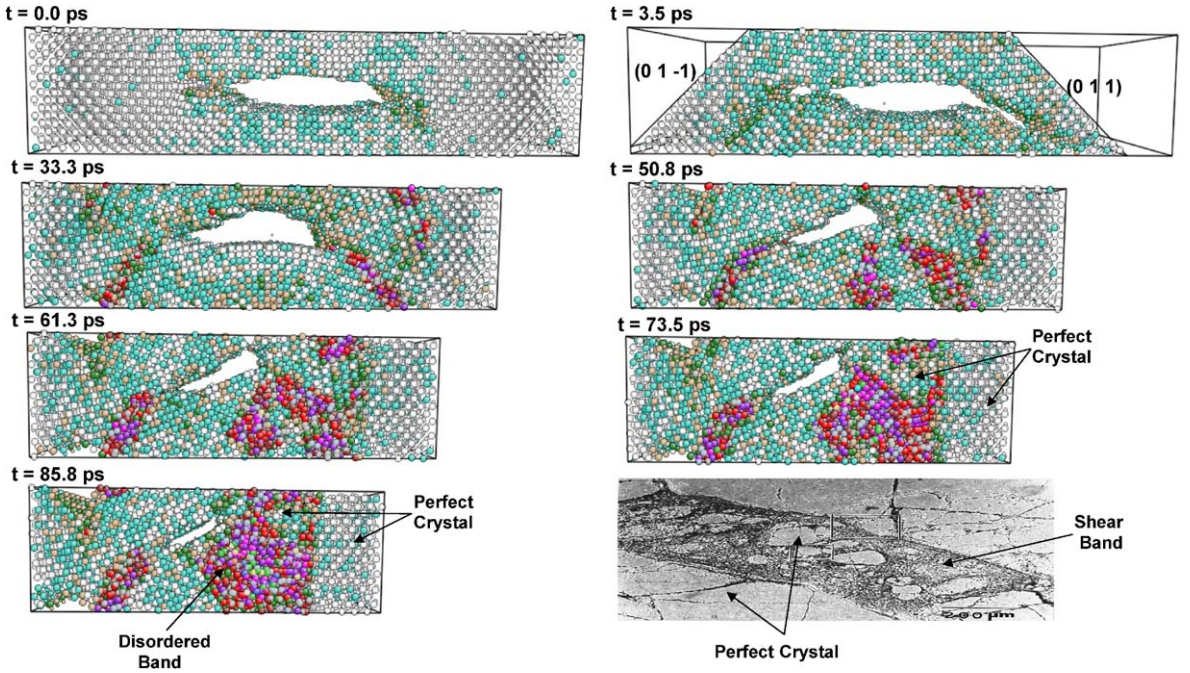

Fig. 3. Analogous plot as in Fig. 2 for specimen with $a_y = 4.75$ Å ($\varepsilon_{yy} = 9.95\%$). Crack opening, with formation of disordered band along open crack surface by attrition and crack bending is shown. Incorporation of perfect crystal pockets into the band is shown at $t = 73.5$ and 85.8 ps. The last snapshot shows experimental results taken from Ref. [9].

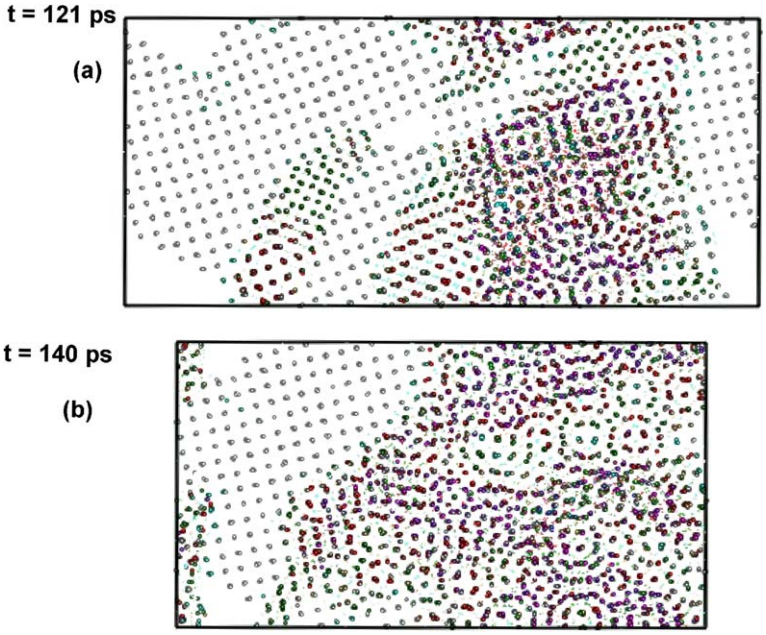

Fig. 4. Snapshots of specimen with $a_y = 4.75$ Å ($\varepsilon_{yy} = 9.95\%$) taken at $t = 121$ and 140 ps. Moire circles are shown to develop inside the disordered band.

process which continues until the end of the simulation, finally transforming the perfect crystal into a highly compressed disordered sample (these final stages are not shown in Fig. 2). During the compression, the crack continuously shrinks. It is interesting to note that after about 53 ps accumulation of shear

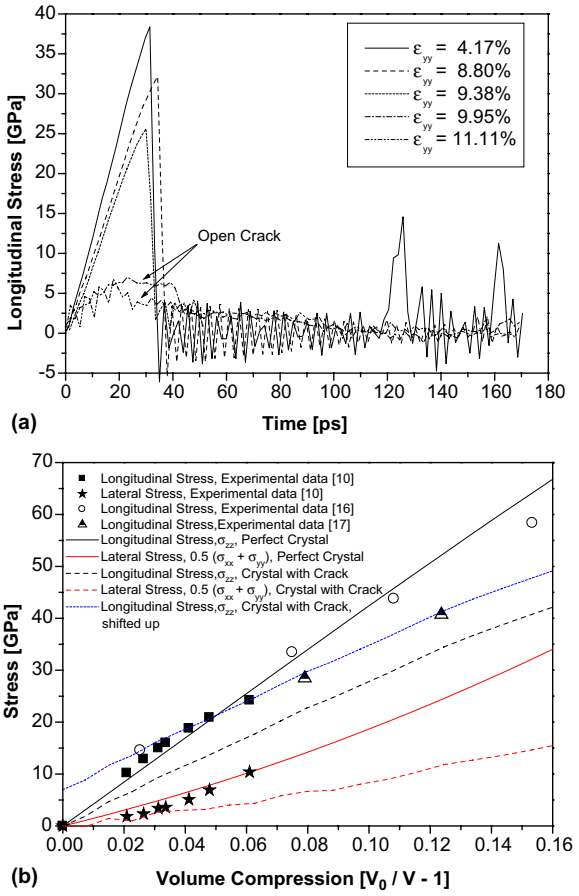

Fig. 5. (a) Calculated longitudinal stress as a function of time for several selections of ε_{yy}. (b) Calculated and measured longitudinal and lateral stress as a function of volume compression.

on the crack-tip side opposite to the growing disordered region and facing the perfect crystal (right side of specimens in Fig. 2), yields crack opening on the (0 1 1) plane and along the [0 −1 1] direction. We acknowledge that this result could be an artefact of the Tersoff potential version used in this study (specifically of the interaction cut-off option employed). Later stages of the deformation show crack closure and extension of the disordered phase (for $t = 77$ ps).

A similar display (seven snapshots) is reported in Fig. 3. In this case, the initial dimensions of the unit cell are $a_x = 4.32$ Å, $a_y = 4.75$ Å, and $a_z = 4.32$ Å, respectively. Thus with respect to the previous case, a slightly larger initial lateral deformation ($\varepsilon_{yy} = 9.95\%$) is applied to the crack to keep it open.

In the first stages of the simulation, crack opening leads to cleavage on the (0 1 1) and (0 1 −1) planes along the [0 −1 1] and [0 −1 −1] directions, respectively. This is shown in the snapshot at $t = 3.5$ ps where the (0 1 1) and (0 1 −1) planes are visualized. Successive compression is shown to produce closure of the cleavage openings with formation of two planar regions containing atoms arranged disorderly which we call hereafter comminuted regions. This process is due to attrition of the atoms located along the open surfaces of the cleavage crack (see snapshot at $t = 33.3$ ps). Bending of the crack, which transforms into a curved slit, is also observed. Therefore the central part of the specimen transforms into a distorted lattice deformed under bending, while the more peripheral regions retain the original lattice orientation.

At longer times, for more extensive compression the comminuted regions become thicker, acting as nucleation sites for the order–disorder transformation. Moreover, a third disordered region is formed via an instability mechanism similar to that reported in Fig. 2 (see snapshot at $t = 50.8$ ps), which originates at the crack surface location where the bending moment (and the shear strain) is highest. This process produces a rotation of the crack whose axis forms an angle of about 45° with the z-axis.

As the compression proceeds the disordered regions continue growing and start to merge (snapshots at $t = 61.3$ ps and $t = 73.5$ ps). Moreover, pockets of atoms retaining the local coordination of the perfect crystal are pushed inside the disordered band (see snapshots at $t = 73.5$ ps and $t = 85.8$ ps). This is more visible in the snapshot at $t = 85.8$ ps where an additional crack is formed which is connected to the slit via a disordered channel and the large disordered band has incorporated a pocket of perfect crystal. The last snapshot is taken from Ref. [9] and shows a similar microstructure observed to form in porous SiC containing particles of ~5 μm size and subject to fast compression. In this case a shear band is created with lumps of micrometer sized perfect crystal debris. Note also that a similar experiment on porous SiC with smaller particles (<1 μm) yielded instead a well bonded shear band without holding perfect crystal detriti, a microstructure similar to that reported in Fig. 2. Therefore a correspondence between SiC particle size (or porosity) and dimension of the initial crack generated in our MD specimen (and thus porosity) is established. Note also that the formation of disordered band via a bending mechanism has been experimentally observed in porous SiC [8] and that the transition from mechanism leading to formation

of a disordered band (process of Fig. 2 or mechanism 1) and that driven by grinding of the open crack surface and bending (process of Fig. 3 or mechanism 2) is sharp in the parameter a_y (ε_{yy}). In fact in our simulations, mechanism 1 occurs provided that $a_y < 4.74$ Å ($\varepsilon_{yy} < 9.72\%$) while, for larger values of a_y (ε_{yy}), the crack opens and mechanism 2 is instead observed.

Finally it is interesting to note that microstructures observed at the micrometer scale obtained compressing SiC at slow rates compared to those attainable in an MD simulation can be reproduced in nanometer size specimen. This is also confirmed in Fig. 4 where we report a different visualization of the disordered band of Fig. 3 taken after $t = 121$ and 140 ps. Fig. 4 shows presence of circular patterns similar to Moire circles [15], which are typically due to the superposition of two slightly misoriented crystal blocks formed by putting a crack under Mode III loading. These patterns are usually observed at larger spatial scales.

Fig. 5 reports the longitudinal stress (σ_{zz}) as a function of time for different initial selections of ε_{yy} (Fig. 5(a)) and the same quantity together with the lateral stress (defined as $0.5\,(\sigma_{xx} + \sigma_{yy})$) as a function of the volume compression $(V(0)/V(t) - 1$, where V is the specimen volume), in Fig. 5(b). Specifically, results for the perfect crystal and the pre-cracked specimen with $\varepsilon_{yy} = 4.17\%$, as well as experimental measurements of shock wave compression tests reported in Refs. [10,16,17] (data from previous work of other investigators is reported by Feng et al. [10]) are shown.

Results in Fig. 5(a) indicate that for cases leading to a type of failure described as mechanism 1, in correspondence with small values of ε_{yy}, the longitudinal stress increases linearly with time as the compression along the z-axis is linearly applied. This trend continues until the disordered band is generated from the crack, when a sharp drop of σ_{zz} sets in, illustrating the sharp transition in time from pre-cracked to failed crystal, similar to a brittle behavior under tension. The calculated peak longitudinal stresses are around 40 GPa for $\varepsilon_{yy} = 4.17\%$, but decrease as a larger tension is orthogonally applied to the crack (for $\varepsilon_{yy} = 9.95\%$, $\sigma_{zz} = 37$ GPa; and for $\varepsilon_{yy} = 9.38\%$, $\sigma_{zz} = 25$ GPa). It is worth remarking that after failure is triggered, material resistance to further compression along the z-axis is lost and oscillations in time of σ_{zz} develop as the transition from ordered to disordered crystal proceeds.

For $\varepsilon_{yy} = 4.17\%$, the longitudinal stress has two peaks around $t = 125$ ps and $t = 163$ ps. These are correlated to the formation of stress-driven crystalline phases with moderate compressional strength ($\sigma_{zz} = 10$–15 GPa), which are stable at large pressures (for example a transformation from zinc-blende to B2 structure is observed).

When the crack is initially opened the material can not withstand large longitudinal stresses. In fact, the peak stresses σ_{zz} are only ~5–7 GPa. Atoms sliding along the open surfaces of the crack, driven by the compressive loading, leading to local bending may be the principal deformation mechanism in this case. This sliding may be the cause of nucleation of local disordered bands on the crack surfaces shown in Fig. 3, a mechanism of attrition which we refer to as comminution.

Results of Fig. 5(b) show that the experimental measurements of longitudinal and lateral stresses can be well reproduced by the present MD simulation. Note that the figure reports MD results for both perfect crystal and pre-cracked SiC. The experimental measurements can be rationalized as follows: during the early stages of deformation the experimental data correlates with those of the perfect crystal. Thus it can be presumed that cracks are not nucleated in the material yet. However, as the compression proceeds some experimental data show a change in slope of the longitudinal stress following a trend more similar to that of the pre-cracked crystal (in Fig. 5(b) we shifted up the longitudinal stress curve obtained by the MD simulation of the pre-cracked specimen and superimposed it on the experimental data in order to show that the simulation reproduces satisfactorily the increase of stress with respect to the volume compression observed experimentally). This suggests that the material cracks and further deformation proceeds with mechanism 1 (note that experimental data in this case correlates better with the MD calculations for the pre-cracked specimen). Similar agreement is obtained for the lateral stress. These results may explain SiC softening observed in shock wave compression experiments via the formation and growth of a localized disordered band, nucleated around cracks.

4. Conclusions

Two deformation mechanisms of pre-cracked SiC under high-rate compression have been revealed by MD simulations. The crack-tip response depends

on the initial level of tension imposed on the crack. At low tension, a disordered band is nucleated from the crack surface in the direction orthogonal to the compression when a critical local atomic shear is reached, after which the longitudinal resistance of the material to compression is lost. The band grows as the compressional force is increased in a manner suggesting a stress-induced transition from an ordered to a disordered phase.

At larger tension the crack remains open and application of a compressional stress yields formation of disordered regions along the boundaries of the opened crack, which grow and merge into a band as the compression proceeds. This process is driven by atomic sliding along the surfaces of the crack and material bending. Moreover, incorporation of fragments of perfect crystal into the disordered band is obtained, in agreement with experimental observations.

Comparison of calculated and measured longitudinal and later stresses as a function of the volume compression indicate that the observed softening of SiC in shock wave compressional experiments may be due to nucleation and growth of localized disordered bands.

Acknowledgments

A.R. and S.Y. thank the Department of Nuclear Science and Engineering, MIT for providing support through the Manson Benedict Fellowship. J.L. acknowledges support by Honda R&D, NSF, AFOSR, ONR, and the Ohio Supercomputer Center.

References

[1] S.I. Vlaskina, K.W. Kim, Y.S. Kim, Y.P. Lee, G.S. Svechnikov, J. Korean Phys. Soc. 31 (1997) 117.
[2] B. Matchen, Applications of ceramics in armor products, in: Advanced Ceramic Materials, 1996, p. 333.
[3] Y.W. Lee, S.C. Lee, H.S. Kim, C.Y. Joung, C. Degueldre, J. Nucl. Mater. 319 (2003) 15.
[4] A.L. Puma, L. Giancarli, H. Golfier, Y. Poitevin, J. Szczepanski, Fusion Eng. Des. 66 & 68 (2003) 401.
[5] C. Degueldre, T. Yamashita, J. Nucl. Mater. 319 (2003) 1.
[6] S. Sarva, S. Nemat-Nasser, Mater. Sci. Eng. A 317 (2001) 140.
[7] F. Lemoine, J. Nucl. Mater. 248 (1997) 238.
[8] C.J. Shih, M.A. Meyers, V.F. Nesterenko, Acta Mater. 46 (1998) 4037.
[9] C.J. Shih, V.F. Nesterenko, M.A. Meyers, J. Appl. Phys. 83 (1998) 4660.
[10] R. Feng, G.F. Raiser, Y.M. Gupta, J. Appl. Phys. 83 (1998) 79.
[11] H. Wang, K.T. Ramesh, Acta Mater. 52 (2004) 355.
[12] M.J. Tang, S. Yip, Phys. Rev. B 52 (1995) 15150.
[13] L.J. Porter, J. Li, S. Yip, J. Nucl. Mater. 246 (1997) 53.
[14] J. Li, Model. Simul. Mater. Sci. Eng. 11 (2003) 173.
[15] W. Bollmann, Crystal Defects and Crystalline Interfaces, Springer-Verlag, Berlin, 1970.
[16] D.A. Crawford, private communication, 1994.
[17] D.E. Grady, M.E. Kipp, SAND92-1832, SANDIA Technical Report, 1993.